Synthesis and characterization of nanostructured and noble metal-based chalcogenide semiconductors

Mengxi Lin

Supervised by Dr. Albert Figuerola Silvestre; Group of Magnetism and Functional Molecules, Department of Inorganic Chemistry, University of Barcelona.

***Abstract*—Platinum containing chalcogenides seem to have bright potential due to the special electrical and catalytic properties stemming from platinum combined with the semiconductor ones of chalcogenides. In this work, a set of synthesis were designed in order to know the influence of different reaction parameters such as temperature, amount of reactants and also different kinds of capping agents on the growth or formation of such nanostructures. The characterization results suggest that a ternary nanostructured chalcogenide system containing two noble metals (Platinum and Silver) was successfully synthesised by using OlAm as capping agent at 120ºC by means of cation exchange reactions. Furthermore, the composition of this ternary is assumed to be Ag_3PtSe_2. As described through this work, the variation on the previously mentioned reaction parameters allows modifying the morphology and composition of this ternary system. Additionally, the possibility of synthesizing nanostructured binary platinum selenide has also been explored.**

***Index Terms*—Nanomaterials: noble metal, platinum, silver selenide nanoparticles, ternary system, binary system.**

I. Introduction

Nanocomposites are a combination of various nanoscale domains sharing a sole interface in such a way that a desired property can be exploited or improved. For instance, silicon nanoparticles (NPs) encapsulated in graphene nanocomposites is responsible for the improvement of cycle performance and rate capability in lithium-ion battery[1], quantum dots contained white-light-diode (LED) shows increase of down-conversion quantum efficiency.[2] and indium-doped GeTe was reported to be a very promising base materials in the thermoelectric devices due to the better electrical conductivity, lower thermal conductivity and enhanced Seebeck coefficient [3],[4]. In order to obtain functional nanocomposites, the most widely used strategy consists first on the synthesis of size-, shape-, structure- and composition-controlled homogeneous NPs made of a sigle material. Then, they will act as precursors in the further synthesis of nanocomposites utilizing bottom-up strategy, where the premade NPs will work as nucleation sites for the second material.

Colloidal nanocrystal synthesis was found to be unique synthesis strategy and this synthesis strategy is in between the solid-state and molecular chemistries. In this synthetic method, the reaction occurs mostly in the solution, where initially the mixture consists of inorganic molecular precursors, amphiphilic surfactants and an organic solvent with high boiling point in order to allow the reaction to be heated at higher temperature. Most importantly, surfactants play a crucial role in this synthetic method: such as solubilizing inorganic molecular precursors in the organic solvent, assisting the growth mechanisms and working as surface stabilizing agents of NPs, rendering them colloidally stable in highly apolar solvents.[5] The colloidal synthetic method can be used to help controlling the size and shape of NPs *e.g.* formation of size-dependent photoluminescent quantum dots,[6] but also to adjust the reactivity of different precursors in order to obtain compositionally complex nanocomposites.[5],[7] Thus, heterostructures can be formed by using colloidal synthesis in different shapes and compositions, which enlarges the variety of properties observed in nanocrystals when combing different materials on one nanostruture. For instance, heterostructured core@shell CdSe@CdTe colloidal nanocrystals belong to the type II-semiconductor heterostructures, in which photovoltaic (PV) performance had been improved with respect to other nanostructures of this nanocrystals [5],[8]

Silver chalcogenides are semiconductor materials with narrow bandgap,[9] which is responsible for the presence of wavelength-tunable absorption in the range of near or middle infrared (NIR or MIR). [10] So that these materials can be applied in the field of infrared optical devices like in photodetectors.[11] Furthermore, silver chalcogenides had also been intensively studied as solid electrolyte materials for the electrochemical applications. For example, they can be used in resistive random access memories due to their high conductivity and super-ionic characteristic.[12],[13] Additionally, a few papers have studied the thermoelectric properties of silver chalcogenides at different temperatures.[14][15] which report that their values of the thermoelectric figure of merit (ZT) can be above 1 at and above 300 K.[16]

Ternary silver chalcogenides including CuAgSe, $AgSbSe_2$ and $AgBiSe_2$ systems exhibit high mobility of Ag *s* electrons,

ultra-low thermal conductivity with great electronic transport ability and high electric conductivity, respectively. [17]–[20] Interestingly, *Dalmases et al*. reported a new ternary Ag_3AuSe_2 alloy that was prepared by using colloidal approaches, which performed much better than the binary Ag-Se system as thermoelectric energy converter.[21]

Platinum dichalcogenides are one of the transition metal dichalcogenides (TMD), which have drawn a lot of attention recently due to their electronic structure. For TMDs from group 10 (Ni, Pd, Pt), the binding energies of valence d-orbitals and valence-p orbitals of the chalcogen atoms are pretty close, so that hybridization between them can occur more extensively in contrast to the TMDs from groups 4-9. [22] Despite platinum diselenide has been proved to be a semimetal in bulk form,[23] it can transformed to semiconductor when decreasing its thickness.[24] Furthermore, platinum dichalcogenide films were verified to have better contact resistivity as top contact in nanoelectronic devices in comparison with conventional ones(Ti and Ni).[25] The possibility of working as electrocatalysts in hydrogen evolution reaction (HER) has also been explored and confirmed.[22] Yet, Pt-based silver chalcogenide ternary materials or pure binary platinum chalcogenides have not been reported so far at the nanoscale, in spite of the interesting electrical and catalytic properties that could be expected.

In this work, a ternary system of Pt-Ag-Se in form of colloidal nanomaterials has been synthesized and characterized using different techniques. Moreover, the possibility of synthesis of pure platinum chalcogenides in colloidal form has also been explored.

II. EXPERIMENTAL SECTION

A. Chemicals

Silver chloride (AgCl, 99.9%), selenium powder (Se, 99.99%), tri-n-octylphosphine (TOP, 97%), and platinum (II) acetylaceto nate ($Pt(acac)_2$, 98%) were purchased from Strem Chemicals. Oleylamine (OLAm, 70%), Octadecene (ODE, 90%), toluene (99.9%), tetraoctylammonium bromide (TOAB, 98 %), tri-n-octylphosphine oxide (TOPO, 99%) were from Sigma-Aldrich. Ethanol (EtOH, 96% v/v) was obtained from Panreac. Acetone (99.8%) was obtained from VWR. Olaylamine and Octadecene were degassed under vacuum for 1 h at 120 ºC before their use in the reactions.

B. Synthesis

1) Synthesis of Ag_2Se NPs.

The synthesis of Ag_2Se followed the procedure reported by Damalses and co-workers. Briefly, 474 mg (6 mmol) of Se and 572 mg (4 mmol) of AgCl were dissolved respectively in 6 mL and 4 mL of TOP in the glovebox. Afterwards, 7.8 g of TOPO and 6.6 mL of OlAm (undegassed) were degassed under vacuum at 120 ºC for 30 min. Then the reaction mixture was heated up to 180 ºC under N_2 atmosphere and the TOP-Se was injected using a plastic syringe into the reaction mixture containing three-neck flask subsequently. As the reaction temperature was back to 180 ºC, the AgCl-TOP was injected quickly. The heating was stopped after 20 min of reaction and the reaction mixture was cooled down. Once the reaction temperature dropped to 50 ºC, 5 mL of toluene was added in order to avoid solidification of TOPO. After all, the solution was washed three times with EtOH, centrifuged 4 min at 4500 rpm. The particles were dispersed in 4 mL of toluene, resulting in a dark brown solution with concentration of 3.6 µmol/L of Ag_2Se.

2) Synthesis of Pt_x-Ag_y-Se_z NPs.

For this synthesis two capping agents have been used.

a) Synthesis using OLAm

The synthesis of Pt_x-Ag_y-Se_z NPS was inspired on the procedure reported by Wolf and his co-workers.[26] The experiment was done in a 25 mL three-neck flask, in which 50.1 mg (0.127 mmol) $Pt(acac)_2$ (Pt:Ag=4:1) was put into the reaction mixture of 7.5 mL of pre-degassed ODE, 100 μL of pre-degassed OlAm and 250 μL Ag_2Se NPs with concentration of 3.6 µmol/L. The whole reaction mixture was degassed under vacuum for another 30 min at room temperature. Then, the reaction atmosphere was changed to N_2 and temperature was increased to 120 ºC. After two and a half hour, the heating was stopped and the solution was cooled down to room temperature. Finally, the solution was washed three times with acetone, centrifuged 10 min at 4500 rpm. The obtained particles were dispersed in 1 mL toluene which showed a brown solution.

In order to optimize experimental results, the same experimental procedures was repeated at 80 ºC and 150 ºC.

b) Synthesis using TOAB

For this part of synthesis, 100 μL of TOAB was used instead of OLAm and the same experimental procedure was repeated at 120 ºC for the same reaction time as *(a)*. Then, in a second experiment, the amount of $Pt(acac)_2$ was reduced in order to decrease the ratio of Pt:Ag down to 24.4 mg (Pt:Ag = 2:1) using however same amount of TOAB at the same temperature for the same reaction time.

3) Synthesis of Pt_xSe_y NPs.

For this synthesis, 50.1 mg (0.127 mmol) $Pt(acac)_2$ was added into the mixture of 4 mL of ODE and 3 mL of OLAm contained in a 25 mL three-neck flask. Then the reaction mixture was degassed under vacuum for 30 min at 120 ºC. Subsequently, the mixture was heated to 200 ºC under N_2 atmosphere and 35.09 mg (0.444 mmol) Se in 1 mL TOP (TOP-Se) was injected. After another hour of reaction at 200 ºC, the heating was stopped and cooled down to the room temperature. The obtained reaction solution (dark brown) was washed three times with acetone, centrifuged 20 min at 4500 rpm. The final product was dispersed in 1 mL toluene, which results in a brown solution.

C. Characterization Methods

1) Transmission Electron Microscopy (TEM)

All the samples were prepared for observation by dilution in toluene, allowed by sonication, deposition and pouring on carbon covered copper TEM grids. The samples were examined by a JEOL 2000 FX II working at 80 kV.

2) X-ray diffraction (XRD)

The spectra were acquired by a PANanalyticalX'Pert Pro MPD Alpha1 diffractometer operating in θ/2θ geometry at 45 kV, 40 mA, and λ= 1.5406 Å (Cu Kα1). Thin layers of the samples were prepared by drop casting and evaporation of the solvent on a monocrystalline Si holder of 15 mm diameter and 0.15 mm height. Scans in the range 2θ =4−100° were run at a step size of 2θ = 0.017 ° and 100 s per step. The data were treated with X'PertHighScore Plus software.

3) High resolution TEM and scanning transmission electron microscopy (STEM) with Energy Dispersive Spectroscopy (EDS)

All the samples were dispersed in toluene, sonicated and deposited on copper TEM grids. They were analyzed using a JEOL JEM-2100 LaB6 transmission electron microscope with energy dispersed analysis of X-rays (EDX), operating at 200 kV in STEM mode using the dark field detector. The spectrometer is an Oxford Instruments INCA x-sight, with Si (Li) detector Map acquisition was accomplished using the INCA Microanalysis Suite version 4.09 software. And the x-ray maps were obtained selecting silver, gold, copper and seleniumas the characteristic x-ray peaks.TEM images were acquired by a Gatan CCD Camera Orius SC1000 and using Digital Micrograh Version 1.71.38

4) Ultraviolet-visible (UV-vis) spectroscopy

The UV-vis Cary 100 Scan 388 Varian spectrophotometer was used with 1 cm path length quartz cuvettes for the UV-vis analysis. The to-be measured samples were diluted in toluene. The UV-vis absorption spectra were recorded on a Perkin Elmer LAMBDA 950 UV-vis spectrophotometer.

III. RESULTS AND DISCUSSION

A. Ag_2Se precursor

The synthesis of Pt-Ag-Se systems start from the preparation of Ag_2Se NPs, which act as precursors and react further with $Pt(acac)_2$ at 120 ºC to obtain the potential ternary Pt-Ag-Se alloyed nanostructures. *Fig. 1 A and B* shows a TEM micrograph of Ag_2Se NPs showing an ordered arrangement of hexagonally-shaped NPs with an average diameter of around 11 nm and their corresponding XRD pattern.

As far as we know, three kinds of stable crystalline polymorphs of Ag_2Se exist, i.e., the semiconducting orthorhombic phase (β-Ag_2Se) with narrow band gap, superionic conducting cubic phase (α-Ag_2Se) and the tetragonal phase (t-Ag_2Se).[27] Among these three phases, the β-Ag_2Se is stable at low temperature and a transition to the α-Ag_2Se requires high temperature which is above 133 ºC.[28] Comparatively, the t-Ag_2Se is only observed at low temperature and it can be found exclusively in the nanocrystals or polycrystalline Ag_2Se contained thin films.[28] For this synthesis, the expected product should be β-Ag_2Se and the result of XRD shown in the *Fig. 1 C* confirms the expectation, which indicates that the NPs contain mainly β-Ag_2Se due to the similarity between the experimental XRD pattern and the reference pattern of β-Ag_2Se. On the other hand, peaks marked with a red star (*)are the most intense peaks from the calculated pattern of t-Ag_2Se [29], which could not be found in the experimental one.

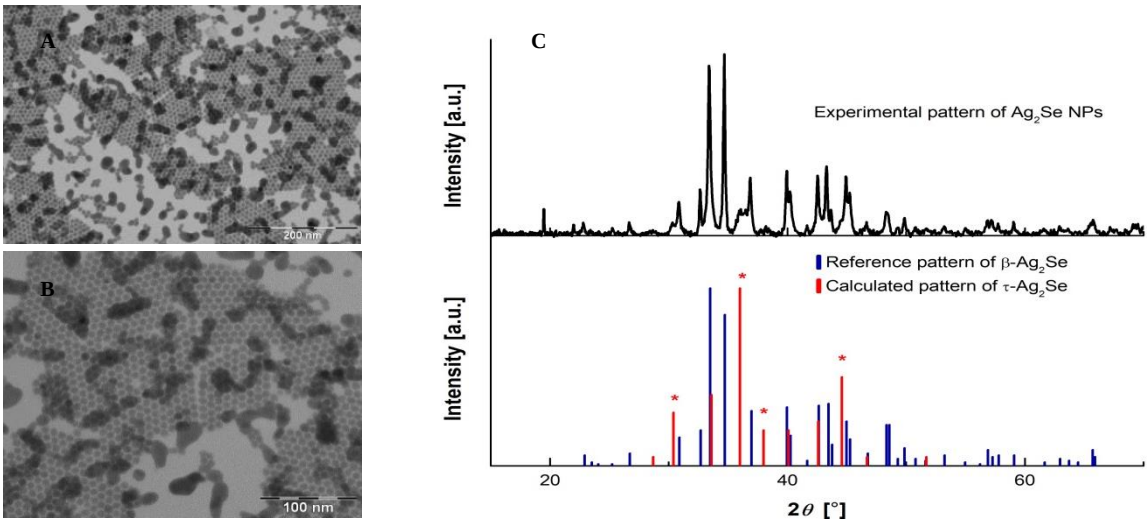

Fig. 1. *(A)and (B): TEM micrograph of synthesized Ag_2Se NPs at different scale bars. (C): Experimental XRD pattern of Ag_2Se NPs (black), reference XRD pattern of $\boldsymbol{\beta}$-Ag_2Se (blue) with reference code JCPSD00-024-1041 and calculated pattern of $\boldsymbol{t}$-Ag_2Se (red).*

TABLE I
EDS PEAK INDENTIFICATION

Element	*Pricinple emision line*	Energy [*Kev*]	Element	*Pricinple emision line*	Energy [*Kev*]	Element	*Pricinple emision line*	Energy [*Kev*]
	$K\alpha_1$	***11.222***		$K\alpha_1$	*22.162*		$K\alpha_1$	*66.832*
	$K\alpha_2$	***11.181***		$K\alpha_2$	*21.990*		$K\alpha_2$	*65.112*
	$K\beta_1$	***12.495***		$K\beta_1$	*24.942*		$K\beta_1$	*75.748*
Se	$L\alpha_1$	***1.379***	***Ag***	$L\alpha_1$	***2.984***	***Pt***	$L\alpha_1$	***9.442***
	$L\alpha_2$	***1.379***		$L\alpha_2$	***2.978***		$L\alpha_2$	***9.361***
	$L\beta_1$	***1.419***		$L\beta_1$	***3.150***		$L\beta_1$	***11.070***
				$L\beta_2$	***3.347***		$L\beta_2$	***11.250***
				$L\gamma_1$	*3.519*		$L\gamma_1$	***12.942***
							M	***2.048***

The theoretical elemental related identification peaks of energy dispersive spectra are presented in the *Table. I.* [30], The emission energy values in bold correspond to the observed emission lines in all spectra through the whole work. According to this, the qualitative and quantitative elemental results obtained for the synthesized precursor (Ag_2Se NPs) have been transferred into *Table. II.* The results indicate that the atomic ratio between silver and selenium is not 2:1 as expected. The two EDS measurements of precursor showed that the atomic ratio of Ag:Se is between 2.5:1 and 3:1. The possible reason for the EDS results could be: (1) Even the EDS measurement can provide both qualitative and quantitative elemental analysis, there is still an error in the measurement. (2): During the reaction, Ag^+ may be partially reduced to metallic Ag and do not participate in the formation of Ag_2Se NPs. Nevertheless, no presence of metallic Ag could be identified in the XRD pattern to confirm this hypothesis, although this could due to the small size of the Ag crystalline domain and the consequent extra wide XRD reflections.[31]

TABLE II
EDS RESULTS OF PRECURSORS

Element		Ag	Se
1_{st} Measurement	Weight %	80.39 ± 1.21	19.61 ± 1.21
	Atomic %	*75.01*	24.99
2_{nd} Measurement	Weight %	*77.66* ± 0.39	22.34 ± 0.39
	Atomic %	*71.79*	28.21

B. Ternary Pt-Ag-Se system

In order to dissolve $Pt(acac)_2$ in an organic solvent and let it react with Ag_2Se NPs without compromising the colloidal stability of the resulting nanocomposite, a kind of complexing and stabilizing agent. In this case, both OLAm and TOAB were tested independently.

1) Tenary Pt-Ag-Se system using OLAm at different temperatures

In this part, the ternary Pt-Ag-Se system was synthesized by using OLAm as both complexing and capping agent at three different temperatures which are 80 ºC, 120 ºC and 150 ºC. Long chain alkylamines possess mild reducing abilities,[32] which a priori could lead to the growth of metallic Pt.

As the TEM micrographs show in *Fig. 2 A-C*, the morphologies of these NPs at different temperatures are quite the same under different temperatures and they all show an aproximately round shape with fluffy surface. The diameter of each NP is around 13 nm. Compared to the morphology of initial Ag_2Se NPs (*Fig. 1*), the hexagonal shape evolved to a more round shape during the experiment and the size has also increased from 11 nm to 13 nm after reacting with Pt(II). Moreover, dark spot in almost each NP could also be noticed on the surface in these three figures , which is assumed to be the Pt domains. The XRD patterns (*Fig. 2 D*) of each sample at different temperature confirm the presence of Pt for the NPs at 120 ºC and 150 ºC. For the NPs at 80 ºC, although the presence of Pt cannot be identified through XRD, the EDS (*Table. III*) results still show a minor presence of Pt. On the other hand, the presence of β-Ag_2Se can be confirmed in the XRD pattern of NPs at 120 ºC and 80 ºC but not for the NPs at higher temperature (150 ºC) , although a minor presence of Se and Ag can also be identified in the EDS results (*Table. III*). The small amount of Se and Ag in the NPs at 150 ºC could also be the reason of non-presence of the Ag_2Se peaks in the XRD.

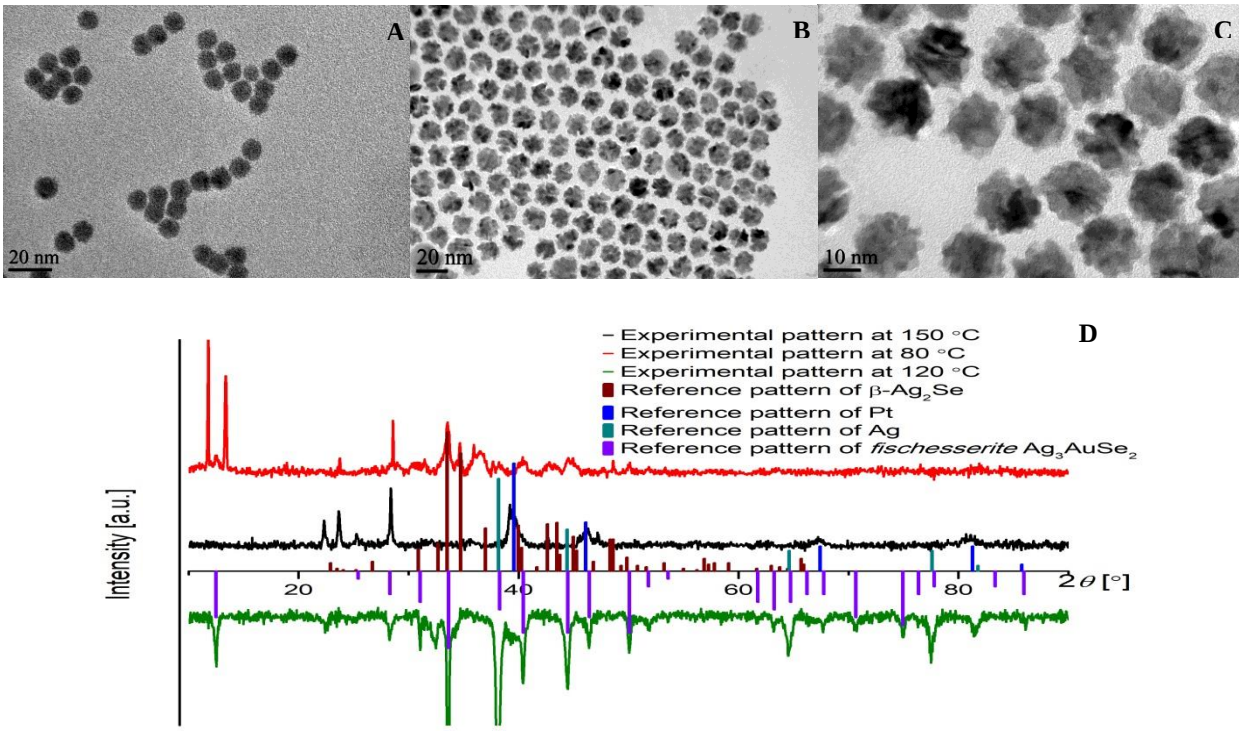

Fig. 2. *TEM micrographs of nanocomposite systems at (A) 80 ºC, (B) at 120 ºC and (C) at 150 ºC. XRD spectrum (D) of the sampleprepared at 80 ºC (red line), NPs at 120 ºC (blue line), NPs at 150 ºC (black line), reference stick pattern of* ***β****-Ag2Se(wine), Pt (navy blue) with reference code JCPDS01-087-0640, Ag (cyan) with reference code JCPDS01-087-0720 and fischeresserite Ag_3AuSe_2 (purple, JCPDS00-025-0367).*

More interestingly, from the sample prepared at 120 ºC contains simultaneously β-Ag_2Se and Pt confirmed by both XRD and EDS (*Table. III and Fig. 2 and 3*) results. Remarkably, some experimental peaks in the XRD cannot be assigned to any of these mentioned phases, which could indicate that besides the formation of Ag_2Se nanocomposites, the Pt precursor might give interacted with the Ag_2Se crystal lattice forming a ternary alloy. However, there is no reference pattern containing these three elements in the database. Surprisingly, in the way of identifying these peaks, we found that they clearly match the XRD reference pattern of Ag_3AuSe_2 *fischeresserite* phase by identifying its most characteristic peak at 12.5 º related to the (110) family of planes with an uncommon relative large interplanar distance, and also by its most intensive peak at 33 º assigned to the (321) family of equivalent planes. This fact suggests that Pt-ion has successfully diffused into the β -Ag_2Se lattice and the transformation from initial orthorhombic phase to the cubic phase occurred during the reaction at 120 ºC. Based on all these data and especially on the structure revealed by XRD we assume that the composition of this ternary system is Ag_3PtSe_2. Under this assumption, the oxidation state of Pt in Ag_3PtSe_2 is Pt (I), which is not a common oxidation state of Pt, but it still exists, [33] and Pt (II) has reduced to Pt(I) during the reaction, in which OLAm could be the reducing agent. Moreover, this composition also indicates that cation exchange between Ag^+ and Pt^+ occurred, leading to the formation of Ag_3PtSe_2. Cation exchange reactions at nanoscale have been increasingly used as a modern post-synthetic method for obtaining novel nanomaterials especially for obtaining the multielemental nanomaterials, which are inaccessible by using direct synthesis methods such as hot injection.[34] The reaction mechanism is simple. For instance, reacting nanocrystal colloids of CdSe with Ag^+ ions in a methanolic solution leads to the formation of Ag_2Se colloids through the cation exchange between Ag^+ in the solution and Cd^{2+} from the host lattice without changing the size and shape of initial ones. [35]

Additionally, analyzing the HRTEM image through fast Fourier transform (*FFT*) of single NP (*Fig. 3*), an interplanar lattice distance of 2.648 Å has been measured and it could be indicative of either the most intense peak (33 º) of Ag_3AuSe_2 related to the (321) set of planes (2.662 Å) or of the (112) family of planes with 2.673 Å of β-Ag_2Se. However, it is hard to discriminate due to the similarity of these three values and further measurement will be necessary.

However, the EDS results (*Table. III and related Fig. 4)* cannot confirm formation of such Ag_3PtSe_2 ternary phase due to the huge amount of Pt and also the incorrect ratio of Se and Ag, which can be respectively explained by two aspects: (1) the presence of huge amount of Pt in the EDS results may be due to the excess of initial amount of $Pt(acac)_2$ in the synthesis of this ternary system (initial ratio of Pt and Ag is 4:1 for the synthesis) and Pt^{2+} ions that have been reduced to metallic Pt by the reducing agent OLAm. (2): the non-ideal ratio of Ag and Se in this ternary system could be due to the same non-ideal ratio of

precursors that has been used for this synthesis. As the EDS results of initial precursors showed before, the amount of Ag exceeds the expected value. Moreover, during the cation exchange reaction, a significant amount of Ag^+ cations would be expelled from the nanocrystal solid lattice to the solution and could easily get reduced to metallic Ag in the presence of OLAm. Indeed, the related XRD pattern in Fig. 2D supports this hypothesis, since most intense peaks of Ag can be identified at 38.2 º and 44.4 º. Therefore, using less reducing conditions in the reaction medium has been considered to avoid the reduction and it will be discussed in the following section.

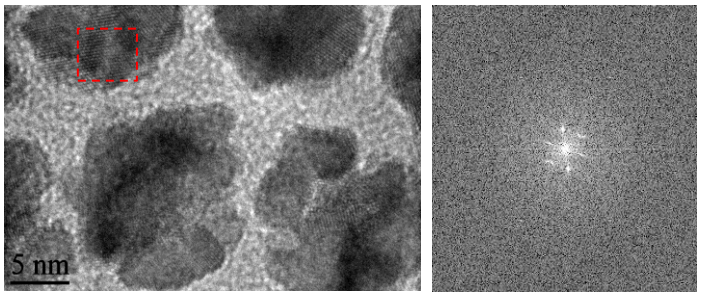

Fig. 3 *HRTEM image of NPs prepared at 120 ºC (left) and corresponding FFT(right).*

TABLE III
EDS RESULTS OF TERNARY SYSTEM AT DIFFERENT TEMPERATURES

At 80 ºC				
Element		**Ag**	**Se**	**Pt**
1st Measurement	Weight %	80.09 ± 0.88	9.95 ± 0.45	9.96 ± 0.85
	Atomic %	*80.75*	13.70	5.55
2nd Measurement	Weight %	*76.5* ± 0.46	18.05 ± 0.33	5.44 ± 0.37
	Atomic %	*73.44*	23.67	2.89
3rd Measurement	Weight %	*78.87 ± 0.99*	13.35 ± 0.61	7.78 ± 0.89
	Atomic %	*77.78*	17.98	4.24
At 120 ºC				
1st Measurement	Weight %	9.04 ± 0.44	1.96 ± 0.35	89.00 ± 0.53
	Atomic %	*14.83*	4.40	80.77
2nd Measurement	Weight %	*10.77* ± 0.37	2.38 ± 0.29	88.85 ± 0.44
	Atomic %	*17.36*	5.23	77.41
At 150 ºC				
1st Measurement	Weight %	3.25 ± 0.77	0.16 ± 0.63	96.59 ± 0.98
	Atomic %	*5.72*	0.39	93.90
2nd Measurement	Weight %	*4.12* ± 0.26	0.56 ± 0.23	95.32 ± 0.34
	Atomic %	*7.15*	1.33	91.52

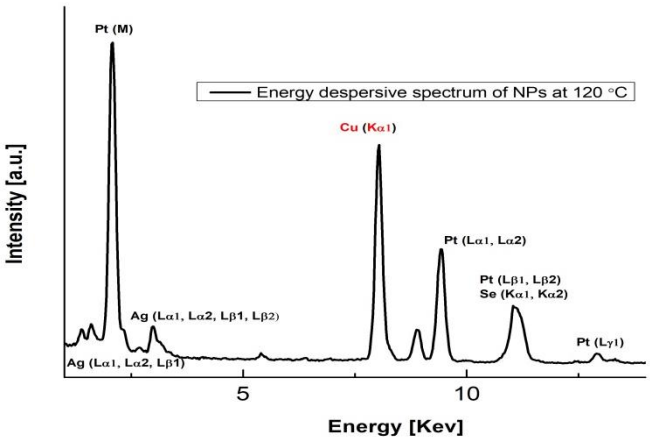

Fig. 4. *Energy dispersive spectrum of the sample prepared at 120 ºC corresponding to the first quantitative results at 120 ºC in the Table. III.*

As we all know, noble metal NPs have been proved to have insightful optical properties manifested by what is called as surface plasmon resonance (SPR), resulting in a significantly strong absorption band in the visible spectrum *e.g.* gold NPs.[36] Although Pt NPs belong to the family of noble metal NPs, they show relatively very low or even no SPR in the visible spectrum due to stronger d-electron excitation comparing to the others, which increase the dielectric constants.[37] Uv-vis spectrum of this ternary Pt-Ag-Se system agrees well with this fact, in which no SPR appears in the range between 400-800 nm. It only presents a continuous absorption which is similar to that of pre-synthesized Ag_2Se NPs (*Fig. 5*).

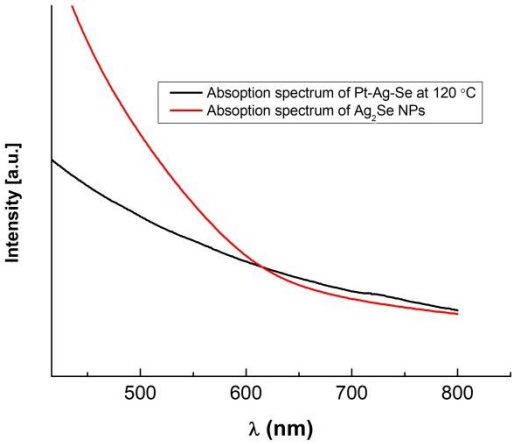

Fig. 5. *UV-vis spectra of Pt-Ag-Se at 120 ºC (black) and Ag_2Se NPs (red)*

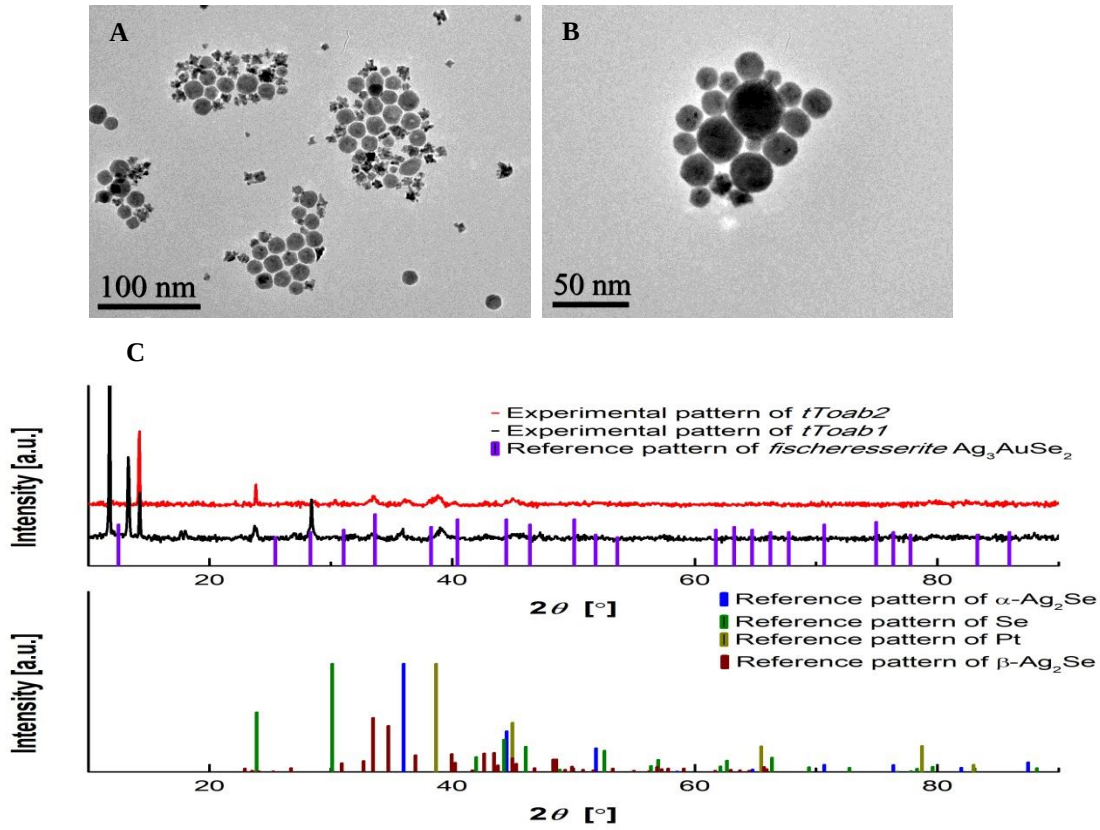

Fig. 6. *TEM micrographs of potential NPs ternary systems at (A) tToab1, (B) tToab2 and XRD spectrum (C) of tToab1 (red line), NPs tToab2(black line), reference stick pattern of* ***β****-Ag_2Se(wine), Pt (yellow), Se (green) with reference code JCPDS01-086-2244, α-Ag_2Se (blue, JCPDS00-076-0135) and fischesserite Ag_3AuSe_2.*

2) Ternary Pt-Ag-Se system using TOAB with different amounts of Pt(acac)$_2$

As mentioned before in the previous section, the used amount of $Pt(acac)_2$ is in a large excess which leads to the large amount of metallic Pt observed in these samples so far. This also makes the determination of the composition of Pt, Ag and Se in the ternary alloy very difficult. Moreover, in the previous synthesis, OlAm was used as both capping agent and reducing agent, which could also be responsible for the large amount of grown metallic Pt and impurifying our samples. Considering all these issues, two approaches have been tested, one with TOAB instead of OlAm as the only capping agent but preserving all other reagents, amounts and conditions with respect to the previous sample prepared at 120 ºC (named *tToab1*). In the other one, TOAB was still used and additionally, the amount of initial $Pt(acac)_2$ was decreased by half, keeping the rest of conditions invariable (named *tToab2*).

As *Fig. 6 A and B* show, the morphologies of these NPs from two approaches (*tToab1*and *tToab2*) are relatively similar, showing an aproximately hexagonal shape. Noteworthily, some star-like particles can be found around and between the hexagonal particles in the both samples, which is suspected to be the metallic Pt. Comparing to the NPs obtained using OLAm, the shape is certainly changed because of different capping agents. As mentioned before, the surface of the NPs using OLAm was pretty fluffy, which hasn't been observed on the surface of NPs using TOAB. Moreover, some white or brighter spots can be also observed on the surface of some NPs in the *tToab1*, which is assumed to be the consequence of Kirkendall effect resulting in the coalescences of some vacancies to form hollow nanostrtuctures, as well will be discussed later

XRD (*Fig. 6 C*) of both samples confirmed the presence of cubic metallic Pt, *β*-Ag_2Se and metallic Se. That means, Se^{2-} has been oxidized, while Pt^{2+} from $Pt(acac)_2$ has been reduced during the reaction. Recalling the whole experimental procedure, TOAB was used only as a capping agent and it is not able to act as a reducing agent because it is a quaternary amine without donating electro pairs unlike OLAm. So there must be something else acting as a reducing agent. One possible explanation of the presence of elemental Se and Pt could be that Pt(II) ions are reduced to Pt by oxidizing Ag_2Se. Moreover, another cubic phase of Ag_2Se also appeared in the XRD pattern, which is uncommon since this phase should be stable at temperature above133 ºC.[28] However, it seems like the cubic crystal system is stabilized by metallic cubic phase. Unfortunately, no *Fischeresserite* peak except the one at ($2\theta = 28.31$ º) was found in the XRD patterns of these two samples, although Ag_2Se and Pt can be identified. So the data do not confirm that the formation of the ternary Pt-Ag-Se

TABLE IV
EDS RESULTS OF TERNARY SYSTEM WITH TOAB

		tToab1		
Element		Ag	Se	Pt
1_{st} Measurement	Weight %	49.25 ± 0.71	21.04 ± 0.52	29.71 ± 0.61
	Atomic %	*52.16*	30.45	17.40
2_{nd} Measurement	Weight %	*48.07* ± 1.74	31.10 ± 1.46	20.83 ± 1.31
	Atomic %	*47.09*	41.62	11.29
		tToab2		
1_{st} Measurement	Weight %	61.48 ± 0.84	25.72 ± 0.69	12.79 ± 0.59
	Atomic %	*59.29*	33.89	6.82
2_{nd} Measurement	Weight %	*59.01* ± 0.65	24.39 ± 0.51	16.60 ± 0.49
	Atomic %	*58.14*	32.82	9.04

system is possible by using TOAB instead of OLAm. In other words, no structural change of initial Ag_2Se is observed from XRD. However, the atomic ratio from EDS results among Ag, Se and Pt has changed a lot compared to the EDS result of initial Ag_2Se and also ternary system using OLAm. First of all, the atomic percentage of Pt has significantly decreased from 95 % to 25 % (*Table. IV, tToab1*) when comparing to the first approach using OLAm because TOAB does not work as reducing agent in this experiment. Moreover, the less Pt (II) has been put into the reaction, the less atomic ratio of Pt contained in the sample. Finally and most surprisingly, the atomic ratio between Ag and Se has also changed a lot from 3:1 in the precursor Ag_2Se NPs sample to 1.5:1, which means the chemical composition of Ag_2Se has changed. As mentioned before, the change of morphology is observed from hexagons of precursor to the hollow structures, which is probably the consequence of Kirkendall effect. This effect was first discovered in the year of 1947 by *Smigelkas* and *Krikendall*, while they were observing the movement of the interface between copper and zinc in brass [38] and it described an unbalanced mutual interdiffusion process of two different metals with different diffusion rates through vacancy exchange, resulting the formation of vacancy at the interface due to the non-equilibrium diffusion kinetics.[39] Moreover, this effect is usually one of the consequences of cation exchange reaction. In our samples, the occurrence of cation exchange together with Kirkendall effect would justify the chemical and morphological change.

Even through the presence of ternary alloyed materials cannot be confirmed when using TOAB, The preliminary characterization data is indicative of morphological and chemical changes. Therefore, further experiments still need to be done.

C. Binary Pt-Se system

In the last part of this thesis, the possibility of synthesizing a binary system of platinum selenide has also been tried. TEM micrographs (*Fig. 7 A and B*) show that the NPs are very small and with non-regular shape compared to the previous Ag_2Se NPs. Although the experimental XRD pattern (*Fig.7 C*) shows relatively broad peaks and the background is very noisy as well, the presence of metallic Se and Pt can still be identified approximately by their most intense peaks respectively which are at 33.58 º and 39.95 º for Se, 39.98 º and 46.25 º for metallic Pt. The EDS measurement (*Table V*) also confirms the presence of these two metals in the NPs and additional provide the roughly quantitative elemental analysis, in which Pt is absolutely dominant in the NPs with around 96 % of atomic proportion compared to the initial ratio of Pt:Se = 1:3.5.

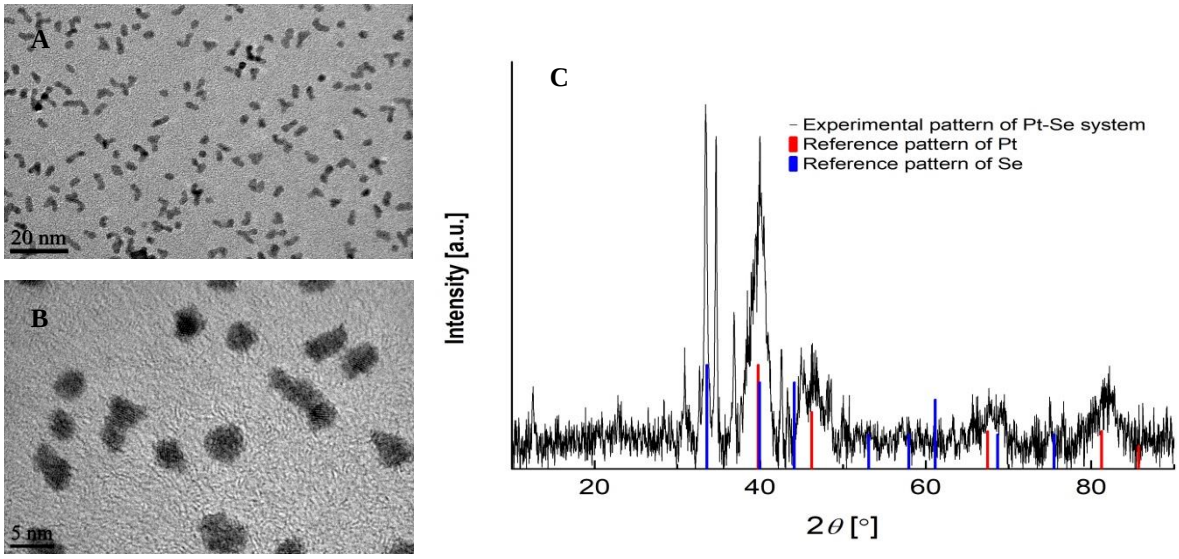

Fig. 7. *(A) and (B): TEM micrographs of potential binary Pt-Se system at different magnifications. (C): Experimental XRD pattern of potential binary Pt-Se system and the reference pattern of Pt with reference code JCPDS01-027-0602 and Se with reference code JCPDS00-027-0602*

TABLE V
EDS RESULTS OF POTENTIAL BINARY PT-SE SYSTEM

Element		Ag	Pt
1_{st} Measurement	Weight %	2.93 ± 0.85	97.07 ± 0.85
	Atomic %	*6.95*	93.05
2_{nd} Measurement	Weight %	*4.65* ± 0.35	95.35 ± 0.35
	Atomic %	*10.25*	89.25

The reason for the appearance of metallic Pt in the sample could relate to the OLAm which had been used as amphiphilic surfanctant and capping agent. The same situation also occurred in the previous synthesis of ternary Pt-Ag-Se system. Besides the presence of Pt, the presence of metallic Se is also found in the XRD. Moreover, Se peaks in the XRD are found to be much narrower than the Pt peaks, which points out that Se crystals are much larger in size, compared to Pt nanocrystals and thus they might distribute differently during the evaporation of the solvent on the grid for EDS measurements. So the EDS measurement may have been performed only on Pt-rich areas where Se is almost completely excluded (*Table V*). Unfortunately, the binary Pt_x-Se system could not be identified in the XRD pattern by going through all the reference patterns.

IV. CONCLUSION

Overall, a series of synthetic approaches at different temperatures, using different capping agents and controlling the amount of reactant have been carried out in order to obtain ternary nanostructured platinum-containing silver selenide systems. Delightedly, this ternary system with round shape and fluffy surface was successfully synthesized by using OLAm as capping agent at 120 ºC, while the product using TOAB has not been confirmed yet. The composition of this ternary system was assumed to be Pt_3AgSe_2 by analogy with the reference XRD data of rare ternary Au_3AgSe_2 *fishesserite* phase used for its identification. Unfortunately, this assumption was not confirmed by the EDS analysis due to several experimental issues. Moreover, the possibility of synthesising a platinum exclusively containing chalcogenide has been also explored without leading to satisfactory results yet. Therefore, the synthesis procedure of ternary system still needs to be optimized for more accurate characterization.

ACKNOWLEDGMENT

This work was part of a project funded by the Spanish Ministry of Science and Innovation. ML is sincerely thankful to Dr. Albert Figuerola as supervisor for thoughtful guidance and insightful discussion throughout this whole work, as well as to the rest of the member of the Group of Magnetic and Functional Molecules for the great support and harmonious working environment. ML is also deeply thankful to parents, partner and friends for their support and care all the time.

REFERENCES

[1] Xiaosi, Z.; Ya-Xia, Y.; Li-Jun, W.; Yu-Guo, G. Self-Assembled Nanocomposite of Silicon Nanoparticles Encapsulated in Graphene through Electrostatic Attraction for Lithium-Ion Batteries. *Advanced Energy Materials* **2012**, *2* (9), 1086–1090.

[2] Cuong, D.; Joonhee, L.; Yu, Z.; Jung, H.; Craig, B.; S., S. J.; Seth, C.; Arto, N. A Wafer-Level Integrated White-Light-Emitting Diode Incorporating Colloidal Quantum Dots as a Nanocomposite Luminescent Material. *Advanced Materials* **2012**, *24* (44), 5915–5918.

[3] Wu, L.; Li, X.; Wang, S.; Zhang, T.; Yang, J.; Zhang, W.; Chen, L.; Yang, J. Resonant Level-Induced High Thermoelectric Response in Indium-Doped GeTe. *NPG Asia Materials* **2017**, *9* (1), 343-7.

[4] Biswas, K.; He, J.; Blum, I. D.; Wu, C. I.; Hogan, T. P.; Seidman, D. N.; Dravid, V. P.; Kanatzidis, M. G. High-Performance Bulk Thermoelectrics with All-Scale Hierarchical Architectures. *Nature* **2012**, *489* (7416), 414–418.

[5] Costi, R.; Saunders, A. E.; Banin, U. Colloidal Hybrid Nanostructures: A New Type of Functional Materials. *Angewandte Chemie - International Edition* **2010**, *49* (29), 4878–4897.

[6] Yu, Y.; Fan, G.; Fermi, A.; Mazzaro, R.; Morandi, V.; Ceroni, P.; Smilgies, D.-M.; Korgel, B. A. Size-Dependent Photoluminescence Efficiency of Silicon Nanocrystal Quantum Dots. *The Journal of Physical Chemistry C* **2017**, *121* (41), 23240–23248.

[7] Buck, M. R.; Bondi, J. F.; Schaak, R. E. A Total-Synthesis Framework for the Construction of High-Order Colloidal Hybrid Nanoparticles. *Nature Chemistry* **2012**, *4* (1), 37–44.

[8] Li, Y.; Mastria, R.; Fiore, A.; Nobile, C.; Yin, L.; Biasiucci, M.; Cheng, G.; Cucolo, A. M.; Cingolani, R.; Manna, L.; et al. Improved Photovoltaic Performance of Heterostructured Tetrapod-Shaped CdSe/CdTe Nanocrystals Using C60 Interlayer. *Advanced Materials* **2009**, *21* (44), 4461–4466.

[9] Junod, P.; Hediger, H.; Kilchör, B.; Wullschleger, J. Metal-Non-Metal Transition in Silver Chalcogenides. *The Philosophical Magazine: A Journal of Theoretical Experimental and Applied Physics* **1977**, *36* (4), 941–958.

[10] Sahu, A.; Khare, A.; Deng, D. D.; Norris, D. J. Quantum Confinement in Silver Selenide Semiconductor Nanocrystals. *Chemical Communications* **2012**, *48* (44), 5458.

[11] Yarema, M.; Pichler, S.; Sytnyk, M.; Seyrkammer, R.; Lechner, R. T.; Fritz-Popovski, G.; Jarzab, D.; Szendrei, K.; Resel, R.; Korovyanko, O.; et al. Infrared Emitting and Photoconducting Colloidal Silver Chalcogenide Nanocrystal Quantum Dots from a Silylamide-Promoted Synthesis. *ACS Nano* **2011**, *5* (5), 3758–3765.

[12] Honma, K.; Iida, K. Specific Heat of Superionic Conductor Ag2S, Ag_2Se and Ag_2Te in α-Phase. *Journal of the Physical Society of Japan* **1987**, *56* (5), 1828–1836.

[13] Simon, R.; Bourke, R. C.; Lougher, E. H. Preparation and Thermoelectric Properties of β-Ag_2Se. *Advanced Energy Conversion* **1963**, *3* (2), 481–505.

[14] Ferhat, M.; Nagao, J. Thermoelectric and Transport Properties of β-Ag2Se Compounds. *Journal of Applied Physics* **2000**, *88* (2), 813.

[15] Conn, J. B.; Taylor, R. C. Thermoelectric and Crystallographic Properties of Ag_2Se. *Journal of The Electrochemical Society* **1960**, *107* (12), 977.

[16] Day, T.; Drymiotis, F.; Zhang, T.; Rhodes, D.; Shi, X.; Chen, L.; Snyder, G. J. Evaluating the Potential for High Thermoelectric Efficiency of Silver Selenide. *Journal of Materials Chemistry C* **2013**, *1* (45), 7568.

[17] Guin, S. N.; Chatterjee, A.; Negi, D. S.; Datta, R.; Biswas, K. High Thermoelectric Performance in Tellurium Free P-Type AgSbSe2. *Energy & Environmental Science* **2013**, *6* (9), 2603.

[18] Ishiwata, S.; Shiomi, Y.; Lee, J. S.; Bahramy, M. S.; Suzuki, T.; Uchida, M.; Arita, R.; Taguchi, Y.; Tokura, Y. Extremely High Electron Mobility in a Phonon-Glass Semimetal. *Nature Materials* **2013**, *12* (6), 512–517.

[19] Han, C.; Sun, Q.; Cheng, Z. X.; Wang, J. L.; Li, Z.; Lu, G. Q. (Max); Dou, S. X. Ambient Scalable Synthesis of Surfactant-Free Thermoelectric CuAgSe Nanoparticles with Reversible Metallic- *n-p* Conductivity Transition. *Journal of the American Chemical Society* **2014**, *136* (50), 17626–17633.

[20] Xiao, C.; Xu, J.; Cao, B.; Li, K.; Kong, M.; Xie, Y. Solid-Solutioned Homojunction Nanoplates with Disordered Lattice: A Promising Approach toward "Phonon Glass Electron Crystal" Thermoelectric Materials. *Journal of the American Chemical Society* **2012**, *134* (18), 7971–7977.

[21] Dalmases, M.; Ibáñez, M.; Torruella, P.; Fernàndez-Altable, V.; López-Conesa, L.; Cadavid, D.; Piveteau, L.; Nachtegaal, M.; Llorca, J.; Ruiz-González, M. L.; et al. Synthesis and Thermoelectric Properties of Noble Metal Ternary Chalcogenide Systems of Ag-Au-Se in the Forms of Alloyed Nanoparticles and Colloidal Nanoheterostructures. *Chemistry of Materials* **2016**, *28* (19), 7017–7028.

[22] Chia, X.; Adriano, A.; Lazar, P.; Sofer, Z.; Luxa, J.; Pumera, M. Layered Platinum Dichalcogenides (PtS2, PtSe2, and PtTe2) Electrocatalysis: Monotonic Dependence on the Chalcogen Size. *Advanced Functional Materials* **2016**, *26* (24), 4306–4318.

[23] Guo, G. Y.; Liang, W. Y. The Electronic Structures of Platinum Dichalcogenides: PtS_2, $PtSe_2$ and $PtTe_2$. *Journal of Physics C: Solid State Physics* **1986**, *19* (7), 995–1008.

[24] Wang, Y.; Li, L.; Yao, W.; Song, S.; Sun, J. T.; Pan, J.; Ren, X.; Li, C.; Okunishi, E.; Wang, Y. Q.; et al. Monolayer $PtSe_2$, a New Semiconducting Transition-Metal-Dichalcogenide, Epitaxially Grown by Direct Selenization of Pt. *Nano Letters* **2015**, *15* (6), 4013–4018.

[25] Yim, C.; Passi, V.; Lemme, M. C.; Duesberg, G. S.; Ó Coileáin, C.; Pallecchi, E.; Fadil, D.; McEvoy, N. Electrical Devices from Top-down Structured Platinum Diselenide Films. *npj 2D Materials and Applications* **2018**, *2* (1), 5.

[26] Wolf, A.; Hinrichs, D.; Sann, J.; Miethe, J. F.; Bigall, N. C.; Dorfs, D. Growth of Cu2-XSe-CuPt and Cu1.1S-Pt Hybrid Nanoparticles. *Journal of Physical Chemistry C* **2016**, *120* (38), 21925–21931.

[27] Wang, J.; Fan, W.; Yang, J.; Da, Z.; Yang, X.; Chen, K.; Yu, H.; Cheng, X. Tetragonal - Orthorhombic - Cubic Phase Transitions in Ag2Se Nanocrystals. *Chemistry of Materials* **2014**, *26* (19), 5647–5653.

[28] Schoen, D. T.; Xie, C.; Cui, Y. Electrical Switching and Phase Transformation in Silver Selenide Nanowires. *Journal of the American Chemical Society* **2007**, *129* (14), 4116–4117.

[29] Sahu, A.; Qi, L.; Kang, M. S.; Deng, D.; Norris, D. J. Facile Synthesis of Silver Chalcogenide (Ag_2E; E = Se, S, Te) Semiconductor Nanocrystals. *Journal of the American Chemical Society* **2011**, *133* (17), 6509–6512.

[30] Shindo, D Oikawa, T. *Energy Dispersive X-Ray Spectroscopy*, 1st ed.; Springer: Tokyo, **2002**.

[31] Jagodzinski, H. H. P. Klug Und L. E. Alexander: X-Ray Diffraction Procedures for Polycrystalline and Amorphous Materials, 2. Auflage. John Wiley & Sons, New York-Sydney-Toronto 1974, 966 Seiten, Preis: £ 18.55. *Berichte der Bunsengesellschaft für physikalische Chemie* **1975**, *79* (6), 553–553.

[32] Wanjala, B. N.; Luo, J.; Loukrakpam, R.; Fang, B.; Mott, D.; Njoki, P. N.; Engelhard, M.; Naslund, H. R.; Wu, J. K.; Wang, L.; et al. Nanoscale Alloying, Phase-Segregation, and Core-Shell Evolution of Gold-Platinum Nanoparticles and Their Electrocatalytic Effect on Oxygen Reduction Reaction. *Chemistry of Materials* **2010**, *22* (14), 4282–4294.

[33] Balch, A. L. Odd Oxidation States of Palladium and Platinum. *Comments on Inorganic Chemistry* **1984**, *3* (2–3), 51–67.

[34] Beberwyck, B. J.; Surendranath, Y.; Paul Alivisatos, A. Cation Exchange: A Versatile Tool for Nanomaterials Synthesis. *Journal of Phsical Chemistry* **2013**, 117 (39), 19759-19770

[35] Son, D. H.; Hughes, S. M.; Yin, Y.; Paul Alivisatos, A. Cation Exchange Reactions in Ionic Nanocrystals. *Science* **2004**, *306* (5698), 1009–1012.

[36] Moores, A.; Goettmann, F. The Plasmon Band in Noble Metal Nanoparticles: An Introduction to Theory and Applications. *New J. Chem.*, **2006**, 30, 1121-1132.

[37] Choi, W. S.; Seo, S. S. A.; Kim, K. W.; Noh, T. W.; Kim, M. Y.; Shin, S. Dielectric Constants of Ir, Ru, Pt, and IrO_2: Contributions from Bound Charges. *Physical Review B* **2006**, *74* (20), 205117.

[38] Nakajima, H. The Discovery and Acceptance of the Kirkendall Effect: The Result of a Short Research Career. *JOM* **1997**, *49* (6), 15–19.

[39] El Mel, A.-A.; Buffière, M.; Tessier, P.-Y.; Konstantinidis, S.; Xu, W.; Du, K.; Wathuthanthri, I.; Choi, C.-H.; Bittencourt, C.; Snyders, R. Highly Ordered Hollow Oxide Nanostructures: The Kirkendall Effect at the Nanoscale. *Small* **2013**, *9* (17), 2838–2843.